Multi-Objective Optimization of Support Structures for Metal Additive Manufacturing

Wadea Ameen Qaid (wadeaameen@gmail.com)
College of Engineering and Architecture https://orcid.org/0000-0003-1542-6680
Abdulrahman Al-Ahmari
King Saud University
Muneer Khan Mohammed
King Saud University
Husam Kaid
King Saud University

Research Article

Keywords: additive manufacturing, electron-beam melting, support structures, overhang structures, optimization

Posted Date: June 15th, 2021

DOI: https://doi.org/10.21203/rs.3.rs-277435/v1

Version of Record: A version of this preprint was published at The International Journal of Advanced Manufacturing Technology on July 12th, 2021. See the published version at https://doi.org/10.1007/s00170-021-07555-9.

Abstract

Electron-beam melting (EBM) is a rapidly developing metal additive manufacturing (AM) method. It is more effective with complex and customized parts manufactured in low volumes. In contrast to traditional manufacturing it offers reduced lead time and efficient material management. However, this technology has difficulties with regard to the construction of overhang structures. Production of overhangs using EBM without support structures results in distorted objects, and the addition of a support structure increases the material consumption and necessitates post-processing. The objective of this study was to design support structures for metal AM that are easy to remove and consume lower support material without affecting the quality of the part. The design of experiment methodology was incorporated to evaluate the support parameters. The multi-objective optimization minimizing support volume, support removal time along with constrained deformation was performed using multi objective genetic algorithm (MOGA-II). The optimal solution was characterized by a large tooth height (4 mm), large tooth base interval (4 mm), large fragmented separation width (2.5 mm), high beam current (6 mm), and low beam scan speed (1200 mm/s).

1. Introduction And Literature Review

EBM is a metal-based AM technology, which works under the powder bed fusion process. It is gaining importance in the field of rapid manufacturing (RM) which is a term used for fast and flexible manufacturing of parts using three-dimensional (3D) computer aided design (CAD) data. The EBM technology was innovated and developed in 1997 by Arcam AB company (Sweden). EBM can produce highly dense parts with mechanical properties similar to or even better than those of parts manufactured via traditional methods. Since it is a powder-bed-fusion process, the parts are built inside the powder envelop. Thus, ideally, the unmelted powder around the part should support the overhanging surfaces, eliminating the need for external support structures. However, the unmelted powder is found to be ineffective to support the molten metal. It is because the unmelted metal powder is not thermally conductive, which leads to dross formation, distortions, and warping [1], [2]. Therefore, the support structures are essential for the successful fabrication of overhanging surfaces [3], [4]. The principal objectives of support structures in AM are 1) the prevention of part curling, distortion, sagging, cracks, shrinkage, and/or other deformations resulting from thermal stresses and 2) anchoring of the part on the building platform [2]. Moreover, they ease the removal of the fabricated part from the built platform and strengthen thin-and-tall parts during the building process. Although support structures are necessary, they pose the following challenges [2], [5]:

- An increased fabrication time and amount of material required.
- Additional effort and a complex process in designing the support.
- The support structures must be removed after the completion of the part building.
- The removal of the support structures introduces risk and can damage the part.

The aforementioned requirements for support structures and the problems associated with the use of support structures must be balanced when considering the placement and design of support structures. In most cases, orientation optimization and implementation of self-supporting rules can minimize the amount of support structure, but it cannot eliminate the support structure. Hence, the optimization of the support structure design is essential in order to minimize the support material and ease the support removal process without affecting the performance of the build. Current support generation methods usually involve the use of certain types of structures to cover the overhang space. These methods may result in the overestimation of the support volume or the placement of a large number of supports, which may be unnecessary and increase the post-processing time [1]. Support structures have many design rules that need to be specified by the designers. For example, the support structures should be designed to engage in minimal contact with the overhang surface parts [6]. Design and optimization of the support structures have received much attention from the researchers. Lindecke et al, 2018, investigated the properties of generating support structures, in laser additive manufacturing. The connection strength between the support structures and the part was evaluated with different support structures design parameters. Based on the analysis of the results a set of design guidelines were suggested [7]. Calignano, 2014, applied the Taguchi method in order to optimize the support structure (design parameters) during selective laser melting (SLM) of overhang and improve the manufacturability of AlSi10Mg and Ti6Al4V overhanging structures.[8]. The effect of support structure design parameters on the part distortions and microstructure during direct metal laser sintering (DMLS) processing of Inconel IN625 alloy parts was investigated by Poyraz [2]. M.X. Gan and C.H. Wong, 2016, investigated three support structure designs manufactured by the SLM process. Out of the 18 intended samples, majority were successfully built except the 'Y' support structures. The fabrication of the 'Y' support structures was aborted due to thermal warpages that obstructed the build process [3]. Zhen-Hong Shen et al, 2016, developed an algorithm for the generation of bridge support structure for 3D printing. The algorithm identify the regions that require support and then determine a set of points that require support based on adaptive sampling, it then selects new bridges through a scoring function, and connects the bridges and model with pillars. Experimentally the generated support was compared with the vertical support and branching support structures. The algorithm was found to save the printing material and time [9]. Similarly, Cheng et al, 2017 developed a general framework based on 3D thermo-mechanical finite element model for the design and optimization of the overhang support structure. The support structure design problem was formulated using the combined minimum energy method and effective heat dissipation method. The finite element model was developed in order to identify the support anchor locations and determine its material usage [1]. Likewise, Rami and Frederic proposed a methodology for designing and optimizing support structures in the EBM process. New support structures were developed and their efficiency was studied. The results showed an enhancement in the efficiency as well as a reduction in geometric defects [10]. Dunbar, 2016, evaluated the mechanical properties of the support structure for laser powder bed fusion AM to obtain information regarding the failure criteria of a support structure. The block type support structure was used with different hatch patterns and its effect on the support strength was evaluated[11]. Zhu et al, 2019, incorporated the tree-supports for the production of overhang structures by fused deposition modeling (FDM). The authors proposed a set of

formulas for stably growing the tree-supports and minimized the support volume using a hybrid of particle swarm optimization method and a greedy algorithm. The results found the combination to be effective in reducing the volume of tree-supports [12]. Zhang et al, 2019, used Taguchi method to analyze the effect of a block support structure (with solid cuboids geometric design parameters) on the part deformation and surface roughness during the fabrication of overhang structures by SLM. The parameters that were considered were; the gap between the upper surfaces of cuboids and the bottom surface of the overhang, the height of the cuboids, the gap between the bottom surfaces of the cuboids and the upper surface of the base, the distance between two adjacent and parallel walls of support structures. The result found that solid pieces or cuboids as support structures can reduce the deformation, but their effects were found to be weaker than those of teeth structures. It was also found that the gap between the cuboids and the overhang has the significant influence on the part deformation and surface quality [13]. It is clear from the literature that the support structures have a significant effect on the precise fabrication of overhang surfaces. Although support strucures are essential during overhang fabrication, they however incur additional time (build and post processing) and additional material comsuption. Most of the published studies have focused on the investigations of support structure for SLS and SLM of overhang surfaces. There is not much work done with regard to the support structure optimization for EBM. In EBM based AM process the feedstock material is in the form of powder which is expensive and since the support material is the same as the build material it results in additional costs. In general the support structures are generated automatically using the software, it is reported that the software sometimes generate inessential support structures. Therefore, investigation of support structures parameters and their effects on the fabricated parts is essential for the design and optimization of the support structures that are easy to remove, consume less material, without having much impact on the quality of the part. In this research the effect of design and process parameters of the fragmented block supports was evaluated and optimized for the fabrication of ledge overhang by EBM using the design of experiments (DOE) and multi-objective optimization genetic algorithm (MOGA-II) technique.

2. Methodology

Fragmented support structures were used in order to reduce the material consumption and enhance the support removal after the built process. They contain two parts: the main support body and a part/support contact area (support teeth). Application of the fragmentation design strategy results in the subdivision of support structures (called fragmented support), where the support walls are divided by slots, as shown in Figure 2a. Fragmented supports have design parameters, such as the separation width, fragmentation interval, and tooth parameters. Figure 2b shows the specimen supports generated in Magics® software (Materialize, Belgium).

The design of the experiment (DOE) methodology was used to conduct experiments and analyze the results systematically. The first step in this method is the identification of the controlled parameters and their levels. The controlled parameters and their respective levels were selected based on the literature survey and screening experiments. Table 1 presents the selected parameters and their respective levels.

Table 1. Fragmented support-structure parameters and levels

Parameter	Level 1	Level 2	Level 3
Tooth height (T_h) (mm)	1	2.5	4
Tooth base interval (T_{bi}) (mm)	1	2.5	4
Fragmented separation width (F_{sw}) (mm)	0.5	1.5	2.5
Beam current (B_C) (mA)	1.5	3.75	6
Beam scan speed (Bss) (mm/s)	1200	1600	2000

Response surface methodology (RSM)-based central composite design was used to perform the experiments systematically. This method is the especially useful in the optimization of responses. According to the parameters and their respective levels, a total of 90 runs were performed (alpha value = 1; 2 replications of factorial points; 16 replications of the center point). Design-Expert version 12 (Statease, Minneapolis) was used to evaluate the effects of different factors on support performance.

2.2. Material and equipment

Ti6Al4V alloy from Arcam AB (Sweden) in powder form with a mean particle diameter of approximately 75 μm was used for fabricating the test specimens. The Ti6Al4V powder composition was Al (5.16 wt.%), V (4.40 wt.%), and Pt (4.01 wt.%), and the remainder Ti, as shown in Figure 2.

An ARCAM A2 machine based on EBM process from ARCAM AB, (Sweden) was used for fabricating the test specimens. The setup and schematic diagram of the EBM process is shown in Figure 3a and 3b respectively. In the EBM process, a high energy electron beam selectively melts the metal alloy powder into a fully solid part in a layer-by-layer manner based on the CAD data [15]. In Arcam machine, the part built parameters vary with that of support structures parameters. In the current study the specimens were built with 50 μm layer thickness using default optimum built parameters supplied by the manufacturer as follows; 200 μm beam spot diameter, 15 mA current, 4530 mm/s scan speed, 3 mA focus offset and 0.1mm line offset. Support design and process parameters were varied based on the Table 1.

In EBM built, parts are surrounded by powder envelop which is then blasted out using powder recovery system with the help of pressurized air. Table 2 presents some of the fabricated specimens after the removal of unmelted powder by the powder recovery system.

Table 2. Specimens fabricated with fragmented support structures

	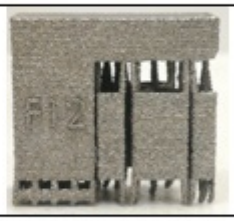	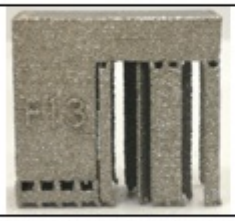	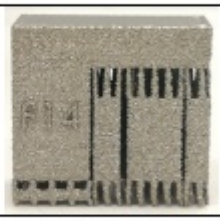
Th=1,Tbi=4,Fsw=0.5, B_c= 6 , B_{ss} = 1200	Th=4,Tbi=4,Fsw=0.5, B_c= 6 , B_{ss} = 1200	Th=1,Tbi=1,Fsw=2.5, B_c= 6 , B_{ss} = 1200	Th=4,Tbi=1,Fsw=2.5, B_c= 6 , B_{ss} = 1200
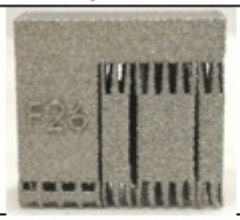		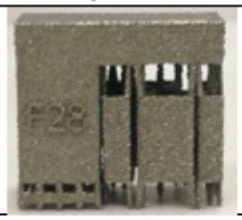	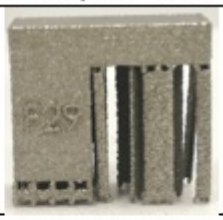
Th=4,Tbi=1,Fsw=0.5, B_c= 6 , B_{ss} = 2000	Th=1,Tbi=4,Fsw=0.5, B_c= 6 , B_{ss} = 2000	Th=4,Tbi=4,Fsw=0.5, B_c= 6 , B_{ss} = 2000	Th=1,Tbi=1,Fsw=2.5, B_c= 6 , B_{ss} = 2000
	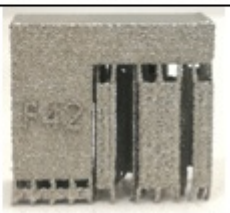	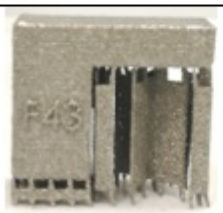	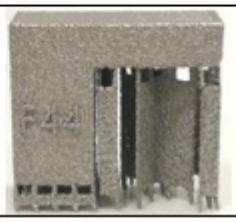
Th=2.5,Tbi=2.5,Fsw=1.5 B_c= 3.75 , B_{ss} = 1200	Th=2.5,Tbi=2.5,Fsw=1.5 B_c= 3.75 , B_{ss} = 2000	Th=2.5,Tbi=2.5,Fsw=1.5 B_c= 3.75 , B_{ss} = 1600	Th=2.5,Tbi=2.5,Fsw=1.5 B_c= 3.75 , B_{ss} = 1600
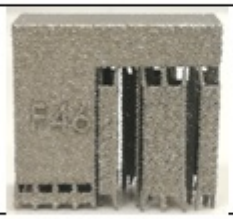	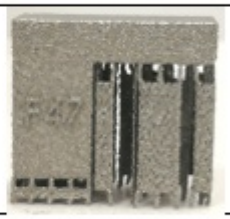		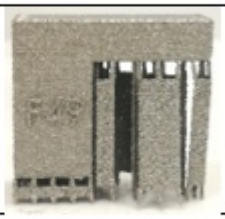
Th=2.5,Tbi=2.5,Fsw=1.5 B_c= 3.75 , B_{ss} = 1600	Th=2.5,Tbi=2.5,Fsw=1.5 B_c= 3.75 , B_{ss} = 1600	Th=2.5,Tbi=2.5,Fsw=1.5 B_c= 3.75 , B_{ss} = 1600	Th=2.5,Tbi=2.5,Fsw=1.5 B_c= 3.75 , B_{ss} = 1600

2.3. Performance measures

Three responses were used to assess the performance of the designed support structures: the support-structure volume, support removal time, and warping deformation. The support-structure volume was measured using an online tool viewstl.com. The support structures were imported into this online application using the browser and their volume was calculated. The support structure removability was evaluated according to the support removal time. The supports were removed manually using wire cutters, and time taken was recorded. To maintain uniformity, the support removal pattern was kept the same for all the specimens The overhang structure deformation was evaluated by measuring the warping deformation. The shadowgraph method, using a profile projector with an accuracy of 2 μm was employed for the measurement of warping deformation as shown in the Figure 4. Shadowgraphy is a quick and useful method for measuring geometric accuracy. In this technique, a two-dimensional representation of a 3D part is created and parts are measured using the optical measurement system.

After the evaluation of performance measures for all the combinations, Analysis of Variance (ANOVA) test was conducted in order to determine the significant parameters, relative effects and study the contribution ratio of the parameters.

Multi objective optimization was performed in order to find the optimal parameters minimizing supports volume, and supports removal time while constraining the warping deformation (WD). The warping deformation was constrained to a very low value using the constrain (WD < 0.1mm). And to ensure the feasibility of the optimal solution by avoiding negative values, another constraint (WD ≥ 0) was added. Multi-objective optimization was then formulated using multi objective genetic algorithm (MOGA-II) and RSM in modefrontier® software (esteco). The workflow for the fragmented support optimization in Mode Frontier software is shown in Figure 5.

To validate the optimization results, the bearing bracket model was designed and fabricated using default and optimum support structures. The bearing bracket is a common component in various aircrafts and it provides a great platform for applying AM. The bracket is intended to be additively manufactured and designed to minimize and/or eliminate the need for support structures. Figure 6 shows the brearing bracket model along with dimensions, support structures region, and build direction.

Two models one with default support structures and other with optimum fragmented support structures were built using EBM. The performance of optimum fragmented support structure was then compared with that of default support structures. Figure 7 shows the bearing bracket model with default fragmented supports and optimum fragmented support structures.

3. Results And Discussion

3.1 Fragmented support volume (FSV)

Results of the ANOVA test at a 95% confidence interval are presented in Table 3. The results showed that the selected fragmented support parameters along with their interactions have significant effect on the support volume. According to the sum of squares the fragmented separation width ($F_{sw.}$) has the most significant effect on the support volume.

Table 3 ANOVA for reduced quadratic model of FSV

Source	Sum of Squares	df	Mean Square	F-value	p-value
Model	4.977E+06	8	6.221E+05	15627.09	< 0.0001
A-Th	5.780E+05	1	5.780E+05	14518.25	< 0.0001
B-Tbi	17848.26	1	17848.26	448.33	< 0.0001
C-Fsw	4.248E+06	1	4.248E+06	1.067E+05	< 0.0001
AB	6050.00	1	6050.00	151.97	< 0.0001
AC	87362.00	1	87362.00	2194.42	< 0.0001
BC	3528.00	1	3528.00	88.62	< 0.0001
B□	248.50	1	248.50	6.24	0.0166
C□	9363.19	1	9363.19	235.19	< 0.0001
Residual	1632.25	41	39.81		
Lack of Fit	1632.25	6	272.04		
Pure Error	0.0000	35	0.0000		
Cor Total	4.979E+06	49			

Figure 8 shows the effect of fragmented support parameters on the fragmented support volume. It was found that as the support tooth height, tooth base interval, and separation width increases, the support volume decreases. The decrease is significant in case of separation width as compared to other parameters. This is becasuse as the fragmented separation width increases, more material is removed from borders and hatches of the support, resulting in lesser support structures and hence the lower support volume as shown in Table 2. The low support volume was achieved with 4 mm T_h, 4mm $T_{bi,}$ and 2.5 mm F_{sw}.

Figure 9 presents the contours plots showing the interaction of fragmented support parameters on the support volume. The contour plot of tooth height and tooth base interval indicate slight interaction and that at lower levels of tooth height the support volume is higher for all levels of tooth base interval. This is because at lower tooth height the perforation at top of the support is small and in the selected range the tooth base interval does not have any significant change in the perforation at low tooth height. The contour plots indicate that the minimum fragmented support volume could be achieved with higher levels of tooth height (factor Th = 4mm), tooth base interval (Tbi = 4 mm) and fragmented separation width (Fws = 2.5 mm).

The mathematical model of the FSV was developed using the response surface methodology (RSM), given by equation 1.1.

FSV =1970.67876 - 123.89379 Th - 28.87730 Tbi - 610.36769 Fsw - 6.11111Th * Tbi + 34.83333 Th * Fsw + 7.00000 Tbi * Fsw +3.67611 Tbi^2 + 50.77126 Fsw^2 (1.1)

The developed predictive model has high R-Square of 99.95% which indicate that the parameters included explain 99.95% of variation in support volume. Therefore, it can be deduced that the developed model is adequate and the predictive model can be utilized for predicting the fragmented support volume.

The developed predictive models were confirmed for their adequacy using a two-sample t-test at a 95% confidence interval. It has been found that P-value for the fitted model is greater than α (0.05). This suggests that null hypotheses H0: μ1= μ2 cannot be rejected i.e., means for actual measured responses and fitted responses are almost equal. A comparison of the actual measured results with predicted ones is shown in Figure 10.

Numerical optimization was then carried out in order to find the optimal parameters minimizing the FSV using desirability approach. The optimization results show several optimal solutions with various desirability values. Table 4 presents five solutions (out of 94), along with their respective desirability values. Figure 11 shows the selected solution by the software. Based on the practical feasibility, the selected solution is acceptable.

Table 4 Samples of optimum solutions for fragmented support volume

#	Th	Tbi	Fsw	FSV	Desirability
1	**3.999**	**3.663**	**2.490**	**535.002**	**1.000**
2	3.925	3.994	2.495	535.982	1.000
3	3.999	3.388	2.500	535.763	1.000
4	4.000	4.000	2.500	530.369	1.000
5	3.987	3.845	2.482	535.730	1.000

The variation of desirability function with tooth height, tooth base interval, and fragmented separation width is shown in Figure 12. It can be seen that the desirability is higher at higher level of selected parameters.

3.2. Fragmented support removal time (FSRT)

ANOVA test was performed in order to evaluate the effect of support parameters on the support removal time. To achieve the normality assumption, transformation (Base 10 Log) was used. It can seen from the Table 5 that most of the selected terms (A, B, C, D, E, BD, DE, B^2) have a significant effect on the FSRT. The main effect plots of the fragmented support removal time are shown in Figure 13. It can be seen that the support removal time decreases with increase in the tooth height, fragmentation separation width, this is because the increase in the tooth height and fragmentation separation width increases the accessibility of the cutting tool (wire cutter). In addition, with increased fragmented separation width the supported area decreases and supports are separated into smaller blocks that are easy to remove, thereby easing the support removal. In case of process parameters, the support removal time was found to have an inverse effect with regard to the beam current and scan speed. As the beam current increases the support removal time increases significantly and as the scan speed increases support removal time decreases. This is due to the fact that at higher beam current, the input energy into the supports is higher, which in turn, increases the support strength thereby increasing the support removal time. Whereas in case of scan speed, it is opposite, higher scan speed results in less input energy and hence lower strength of the supports and lower removal times.

Table 5 ANOVA for reduced quadratic model of Log FSRT

Source	Sum of Squares	df	Mean Square	F-value	p-value
Model	20.25	8	2.53	107.62	< 0.0001
A-Th	0.5925	1	0.5925	25.19	< 0.0001
B-Tbi	0.2390	1	0.2390	10.16	0.0020
C-Fsw	0.4476	1	0.4476	19.03	< 0.0001
D-Bc	15.61	1	15.61	663.45	< 0.0001
E-Bss	2.34	1	2.34	99.54	< 0.0001
BD	0.1793	1	0.1793	7.62	0.0071
DE	0.3557	1	0.3557	15.12	0.0002
B	0.4896	1	0.4896	20.82	< 0.0001
Residual	1.91	81	0.0235		
Lack of Fit	1.15	34	0.0339	2.11	0.0090
Pure Error	0.7542	47	0.0160		
Cor Total	22.16	89			

The interactions of the fragmented support parameters on the FSRT is shown in Figure 14. It was found that at lower levels of tooth base interval and scan speed, FSRT increases significantly with increase in beam current. This is because at lower levels of scan speed the input energy is higher for every level of beam current resulting in stronger support structures that are difficult to remove. The FSRT was found to be minimum with low beam current and that at low beam currents variation of tooth base interval and scan speed did not had any significant effect on FSRT.

The predictive model of FSRT is is given by the equation 1.2.

Log (FSRT) = 1.27196 - 0.063166Th + 0.389343Tbi - 0.082355Fsw + 0.122791Bc - 0.000781Bss - 0.015681Tbi * Bc + 0.000083Bc * Bss - 0.074131Tbi² (1.2)

The developed model has R –Square value of 91.40%. The high R-square value confirms the model adequacy and that all factors affecting FSRT have been considered in the predictive model. T-test of 95% confidence interval was conducted between actual and predicted data and it was found that P-value for the fitted model is is greater than α value (α= 0.05). This suggests that null hypotheses H0: μ1= μ2 cannot be rejected i.e., means for actual measured responses and fitted responses are almost equal. A comparison of the measured results with predicted ones is shown in Figure15.

To find the optimal solution minimizing the FSRT, numerical optimization was then performed using desirability approach. Five of the optimal solutions (out of 100 solutions) are listed in Table 6. Figure 16 shows the selected solution based on the software suggestions, it was found to conflict with warping deformation response. The variation of desirability function with the support parameters is shown in Figure 17. The desirability was found to be high for low beam current and higher levels of tooth base interval and beam speed.

Table 6 Samples of optimum solutions for fragmented support removal time

#	Th	Tbi	Fsw	Bc	Bss	SRT	Desirability
1	**3.468**	**3.995**	**2.499**	**1.500**	**1976.31**	**1.000**	1
2	3.903	3.989	2.384	1.590	1996.606	1.000	1
3	3.604	3.977	2.398	1.503	1993.304	1.000	1
4	3.998	1.041	2.450	1.502	1999.891	1.000	1
5	3.844	1.008	2.457	1.506	1970.917	1.000	1

3.3. Warping deformation with fragmented support (WDFS)

The effects of the design and process parameters of fragmented support on the overhang warping deformation was evaluated and analyzed using the ANOVA test. Table 7 presents the ANOVA test results of the WDFS. The results show that the selected parameters along with few interaction terms have significant effect on the WDFS.

Table 7 ANOVA for Reduced cubic model of warping deformation with fragmented support

Source	Sum of Squares	df	Mean Square	F-value	p-value
Model	6.99	18	0.3885	47.82	< 0.0001
A-Th	0.1791	1	0.1791	22.05	< 0.0001
B-Tbi	0.1837	1	0.1837	22.62	< 0.0001
C-Fsw	0.1665	1	0.1665	20.49	< 0.0001
D-Bc	4.41	1	4.41	543.50	< 0.0001
E-Bss	0.4687	1	0.4687	57.70	< 0.0001
AB	0.0558	1	0.0558	6.87	0.0107
AC	0.0347	1	0.0347	4.28	0.0423
AD	0.0002	1	0.0002	0.0303	0.8622
BC	0.0034	1	0.0034	0.4181	0.5200
BD	0.0886	1	0.0886	10.90	0.0015
BE	0.0057	1	0.0057	0.7064	0.4035
CD	0.1269	1	0.1269	15.62	0.0002
CE	0.0047	1	0.0047	0.5789	0.4492
DE	0.3844	1	0.3844	47.33	< 0.0001
D	0.5861	1	0.5861	72.15	< 0.0001
ABD	0.0902	1	0.0902	11.11	0.0014
BCD	0.0783	1	0.0783	9.64	0.0027
BCE	0.1206	1	0.1206	14.85	0.0003
Residual	0.5767	71	0.0081		
Lack of Fit	0.5254	24	0.0219	20.08	< 0.0001
Pure Error	0.0513	47	0.0011		
Cor Total	7.57	89			

The main effect plots of the WDFS are shown in Figure 18. The WDFS increases with increase in tooth height, tooth base interval, fragemeted separation width, and scan speed. Whereas it decreases with increase in beam current. The effect is however significant in case of beam current as compared to other

parameters. The increase in the tooth height, tooth base interval results in weaker contact between the support and part which inturn results in deformation. Increase in fragmented separation width increases the offset distance between the fragmented supports thereby increasing the unsupported area and resulting in increased deformation. Low beam, and high scan speed results in weaker supports due to lower input energy which in turns causes higher deformation. The contour plots showing the interactions of the fragmented support parameters on the WDFS are shown in Figure 19. The variation of deformation was found to be higher with beam current especially at high levels of fragmented separation width and tooth base interval as compared to the lower levels.The interaction of tooth height and fragmented separation width reveal insignificant variation of deformation with varying tooth height especially when the fragmented separation width is below 2mm.

The predictive model of the warping deformation achieved by the backward elimination method is is given by the equation 1.3.

WDFS = -0.577325 + 0.111608 Th + 0.261658 Tbi + 0.231394 Fsw - 0.184232 Bc + 0.000733 Bss -0.040943 Th * Tbi +0.015531 Th * Fsw - 0.017962 Th * Bc - 0.072031 Tbi * Fsw -0.014017 Tbi * Bc -0.000093 Tbi * Bss + 0.006124 Fsw * Bc - 0.000159 Fsw * Bss - 0.000086 Bc * Bss + 0.036045 Bc^2 + 0.007417 Th * Tbi * Bc - 0.010366 Tbi * Fsw * Bc + 0.000072 Tbi * Fsw * Bss (1.3).

The developed model has R –Square value of 92.32%, which confirms the model adequacy. T-test of 95% confidence interval was performed between the actual and predicted data. It was found that the P-value for the fitted model is greater than α value (α= 0.05) which suggests that null hypotheses H0: μ1= μ2 cannot be rejected i.e., means for actual measured responses and fitted responses are almost equal. A comparison of the actual measured results with predicted ones is shown in Figure 20.

Optimization was then carried out using desirability approach in order to find the optimal parameters minimizing the WDFS. Five of the optimal solutions (out of 100 solutions) are listed in Table 8. Based on the practical feasibility the suggested solution is applicable with acceptable values for the other responses. Figure 21 shows the selected solution based on software suggestions. The variation of desirability function with the support parameters is shown in Figure 22.

Table 8 Optimum Parameters for warping deformation with fragmented support

#	Th	Tbi	Fsw	Bc	Bss	WDFS	Desirability
1	**2.035**	**2.165**	**0.876**	**4.958**	**1340.552**	**0.000**	**1**
2	2.720	1.234	0.997	4.797	1385.761	0.000	1
3	1.407	1.334	1.071	5.021	1715.529	0.000	1
4	1.326	1.045	0.586	4.941	1806.601	0.000	1
5	1.064	3.069	1.201	5.231	1281.563	0.000	1

3.4. Multi-response optimization of fragmented support

The results of multi-response optimization of the fragmented support are presented in bubble charts in Figure 23 and Figure 24. The 3D bubble chart is plotted using the design points against the two objective

functions i.e. fragmented support volume (FSV) and fragmented support removal time (FSRT), where one of the output variables i.e. warping deformation (WDFS) is represented by the diameter of the bubbles. Design points present in the original DOE matrix are real whereas predicted ones from RSM are virtual, also the feasible design points have a gray color whereas the unfeasible design points have a yellow color (Figure 23). As the objective of the optimization problem is to minimize the fragmented support volume (FSV) and fragmented support removal time (FSRT), the feasible design points corresponding to the lower-left corner of the bubble chart (inside the red rectangular) are the candidates for the optimal solution Figure 24.

Table 9 presents the optimum solutions; The first solution is the real and corresponds to the original DOE matrix. The optimal solution consists of high levels of parameters except for the scan speed.

Table 9 Optimal solutions mimizing fragmented support volume, and support removal time

#	Th (mm)	Tbi (mm)	Fsw (mm)	Bc (mA)	Bss (mm/s)	FSV (mm^3)	FSRT (S)	FSDW (mm)
1	**4**	**4**	**2.5**	**6**	**1200**	**536**	**10**	**0.094000**
2	3.5	4	2.5	6	1400	562.3	12.25	0.091536
3	4	3.5	2.5	6	1400	541.17	12.37	0.095600

Another way to analyze the design points is to use a parallel coordinate chart as shown in Figure 25. A parallel coordinate chart can show design points with all the parameters used in the study. In summary, optimum results were found with high tooth height, high tooth base interval, high fragmented separation width, high, beam current, and low beam scan speed.

The optimal fragmented support parameters were applied to the selected bearing bracket design in order to validate the optimization. The results show that the application of optimum fragmented support structures (from multi-response optimization) resulted in the decrease in support structures volume, the un-melted powder removal time, and the support removal time at the expense of around 50 µm warping deformation as shown in Figure 26. The optimum fragmented support structures resulted in the reduction of the support volume by 36%, powder removal time by 66%, and support removal time by 72%. Therefore there is a significant reduction in material consumption, and post processing time at the expense of low level of warping deformation of around one layer (50 µm).

4 Conclusions

The objective of this study was to design support structures for metal AM that allow the production of parts that are easy to remove, consume less material without having much impact on the quality of the part. The analysis of results showed that the design and process parameters of the support structures significantly affect their performance. Support structures with the tooth height of 4 mm, tooth base interval of 4 mm, fragmented separation width of 2.5 mm and specific process parameters (beam current

of 6 mA and beam scan speed of 1200 mm/s) yielded favorable results for material consumption, support removability, and part quality.

Based on the analysis of the results, the following conclusions can be drawn:

- The fragmented separation width and the tooth height have the most significant effect on the fragmented support volume.
- The combination of a tooth height of 3.999mm, a tooth base interval of 2.663mm, and fragmented separation width of 2.490 mm resulted in the optimum fragmented support volume (535.002mm^3).
- The beam current (Bc) and the beam scan speed have the most significant effect on the fragmented support removal time FSRT.
- The combination of a tooth height of 3.468mm, a tooth base interval of 3.995 mm, a fragmented separation width of 2.499mm, a beam current of 1.5mA and beam scan speed 1976 mm/s resulted in the optimum fragmented support removal time (1s).
- The beam current (Bc) and the beam scan speed have a significant effect on the warping deformation with fragmented support (WDFS).
- The optimum combination of (Th of 2.035mm, Tbi of 2.165mm, Fsw of 0.876mm, Bc of 4.958mA and Bss 1340.552 mm/s) resulted in the reduction of FSV by 18% and 89% in FSRT without any warping deformation.
- The combination of a tooth height of 4mm, a tooth base interval of 4mm, a fragmented separation width of 2.5mm, a beam current of 6mA and beam scan speed 1200 mm/s resulted in minimum fragmented support volume (536. mm^3), minimum fragmented support removal time (10s), and minimum warping deformation (0.094mm).

The EBM process is relatively new and is still in the development stage; therefore, it provides many research opportunities in different aspects. Regarding the design of support structures for EBM, optimization of tree support structures is suggested for future research.

Declarations

Funding : The authors are grateful to the Raytheon Chair for Systems Engineering for funding.

Conflicts of interest

The authors declare no conflicts of interest.

Availability of data and material**:** All data generated or analysed during this study are included in this published article (and its supplementary information files).

Code availability: 'Not applicable'

Author Contributions: Wadea Ameen and Abdulrahman M. Al-Ahmari conceived and designed the study. Wadea Ameen and Muneer Khan Mohammed conducted the experiments, analyzed the results, wrote the manuscript and reviewed it. Abdulrahman Al-Ahmari reviewed and supervised the work.

References

[1] Cheng B, Chou YK. Overhang Support Structure Design for Electron Beam Additive Manufacturing. ASME 2017 12th International Manufacturing Science and Engineering Conference collocated with the JSME/ASME 2017 6th International Conference on Materials and Processing: American Society of Mechanical Engineers; 2017. p. V002T01A18-VT01A18.

[2] Ö. Poyraz* EY, G. Akbulut*, A.Orhangül*, S. Pilatin*. INVESTIGATION OF SUPPORT STRUCTURES FOR DIRECT METAL LASER SINTERING (DMLS) OF IN625 PARTS. International Solid Freeform Fabrication Symposium. Austin, Texas, USA2015.

[3] Gan M, Wong C. Practical support structures for selective laser melting. Journal of Materials Processing Technology 2016;238:474-84.

[4] Zeng K. Optimization of support structures for selective laser melting: University of Louisville; 2015.

[5] Järvinen J-P, Matilainen V, Li X, Piili H, Salminen A, Mäkelä I, et al. Characterization of effect of support structures in laser additive manufacturing of stainless steel. Physics Procedia 2014;56:72-81.

[6] Jhabvala J, Boillat E, André C, Glardon R. An innovative method to build support structures with a pulsed laser in the selective laser melting process. The International Journal of Advanced Manufacturing Technology 2012;59:137-42.

[7] Lindecke PNJ, Blunk H, Wenzl J-P, Möller M, Emmelmann C. Optimization of support structures for the laser additive manufacturing of TiAl6V4 parts. Procedia CIRP 2018;74:53-8.

[8] Calignano F. Design optimization of supports for overhanging structures in aluminum and titanium alloys by selective laser melting. Materials & Design 2014;64:203-13.

[9] Shen Z-H, Dai N, Li D-W, Wu C-Y. Bridge support structure generation for 3D printing. Materials, Manufacturing Technology, Electronics and Information Science (MMTEI2015) Proceedings for the 2015 International Workshop on Materials, Manufacturing Technology, Electronics and Information Science (MMTEI2015)2016. p. 141-9.

[10] RamiTOUNSI FV. New concept of support structures in Electron Beam Melting manufacturing to reduce geomtricdefects. 15e Colloque National AIP-Priméca2017.

[11] Dunbar AJ. Analysis of the laser powder bed fusion additive manufacturing process through experimental measurement and finite element modeling: The Pennsylvania State University; 2016.

[12] Zhu L, Feng R, Li X, Xi J, Wei X. A Tree-Shaped Support Structure for Additive Manufacturing Generated by Using a Hybrid of Particle Swarm Optimization and Greedy Algorithm. Journal of Computing and Information Science in Engineering 2019;19:041010.

[13] Zhang K, Fu G, Zhang P, Ma Z, Mao Z, Zhang D. Study on the Geometric Design of Supports for Overhanging Structures Fabricated by Selective Laser Melting. Materials 2019;12:27.

[14] Thomas D. The development of design rules for selective laser melting: University of Wales; 2009.

[15] Cheng B, Chou K. Deformation Evaluation of Part Overhang Configurations in Electron Beam Additive Manufacturing. ASME 2015 International Manufacturing Science and Engineering Conference: American Society of Mechanical Engineers; 2015. p. V001T02A72-VT02A72.

[16] Vora P, Derguti F, Mumtaz K, Todd I, Hopkinson N. Investigating a Semi-Solid Processing Technique Using Metal Powder Bed Additive Manufacturing Processes. 24th Annual International Solid Freeform Fabrication Symposium-An Additive Manufacturing Conference, Austin, TX, USA2013.

[17] Cheng B, Lu P, Chou K. Thermomechanical Investigation of Overhang Fabrications In Electron Beam Additive Manufacturing. ASME 2014 International Manufacturing Science and Engineering Conference collocated with the JSME 2014 International Conference on Materials and Processing and the 42nd North American Manufacturing Research Conference: American Society of Mechanical Engineers; 2014. p. V002T02A24-VT02A24.

[18] Vayre B, Vignat F, Villeneuve F. Identification on some design key parameters for additive manufacturing: application on electron beam melting. Procedia CIRP 2013;7:264-9.

Figures

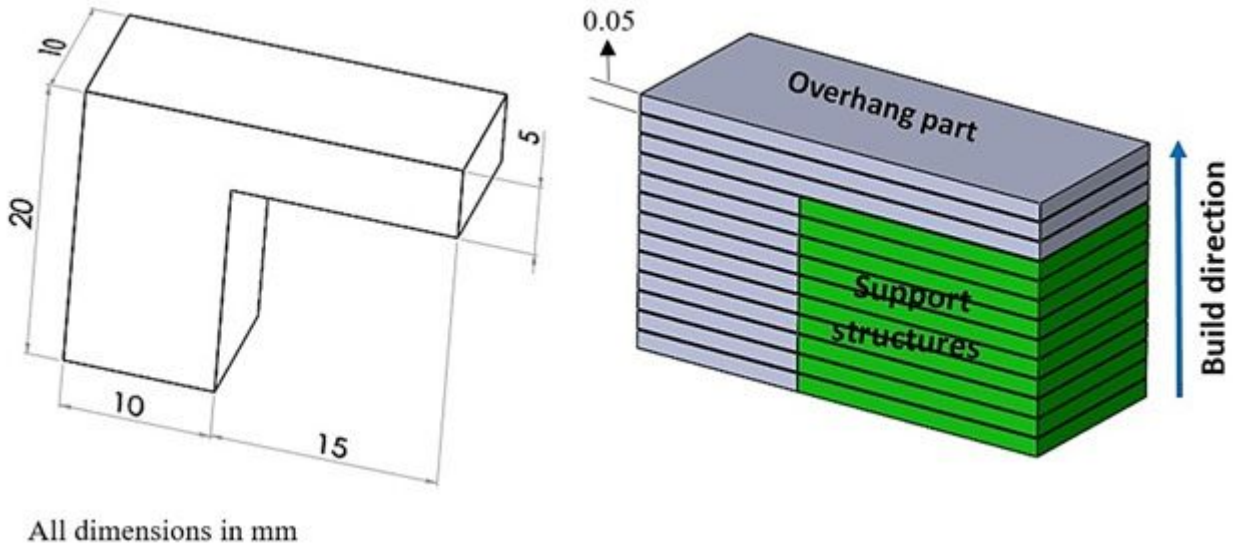

Figure 1

Ledge overhang geometry showing layer thickness and build oreintation

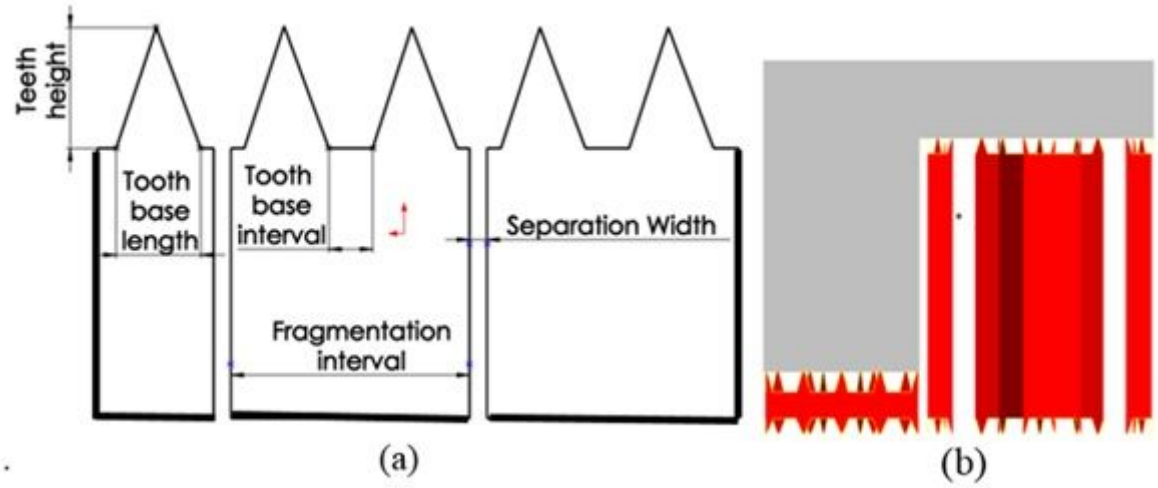

Figure 2

Fragmented support structures a) design parameters b) specimen supports generated in Magics® software

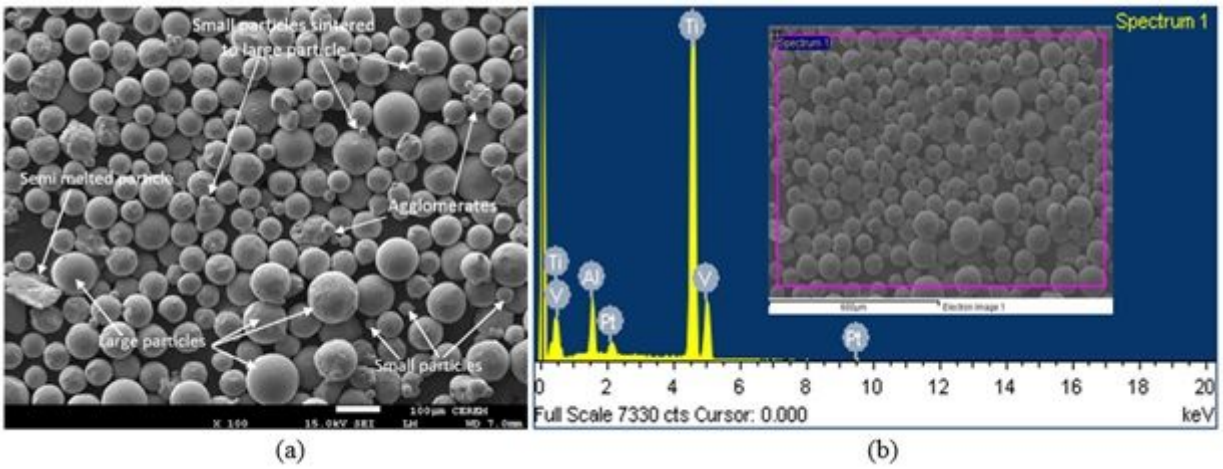

Figure 3

Ti6Al4V feedstock material: a) scanning electron microscopy image b) energy-dispersive X-ray spectroscopy results

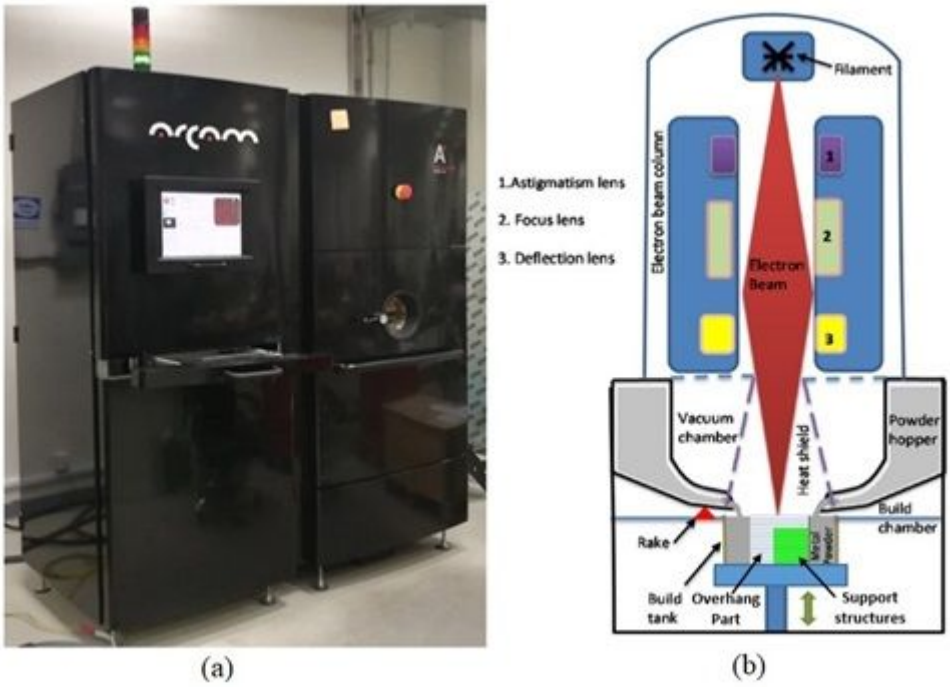

Figure 4

(a) ARCAM A2 machine used in the study (b) schematic diagram of EBM process

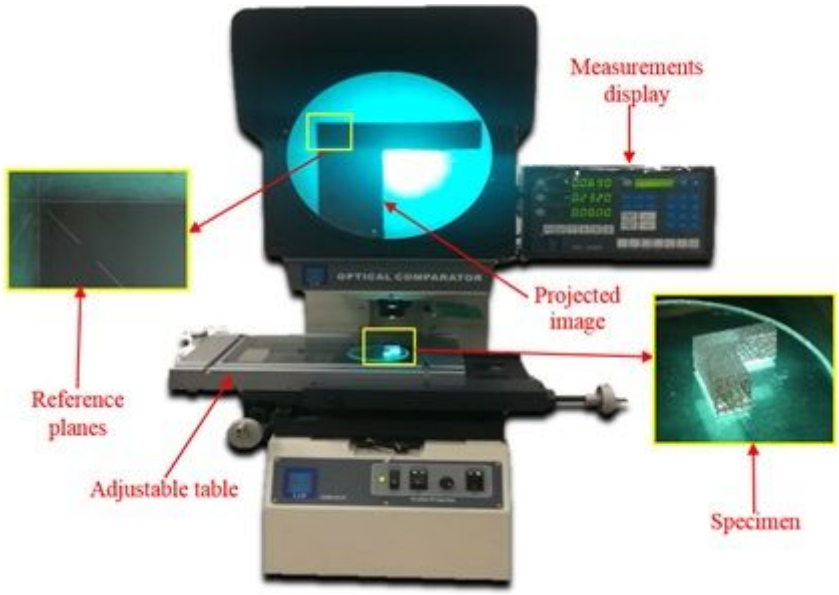

Figure 5

Profile projector used for the measurement of warping deformation

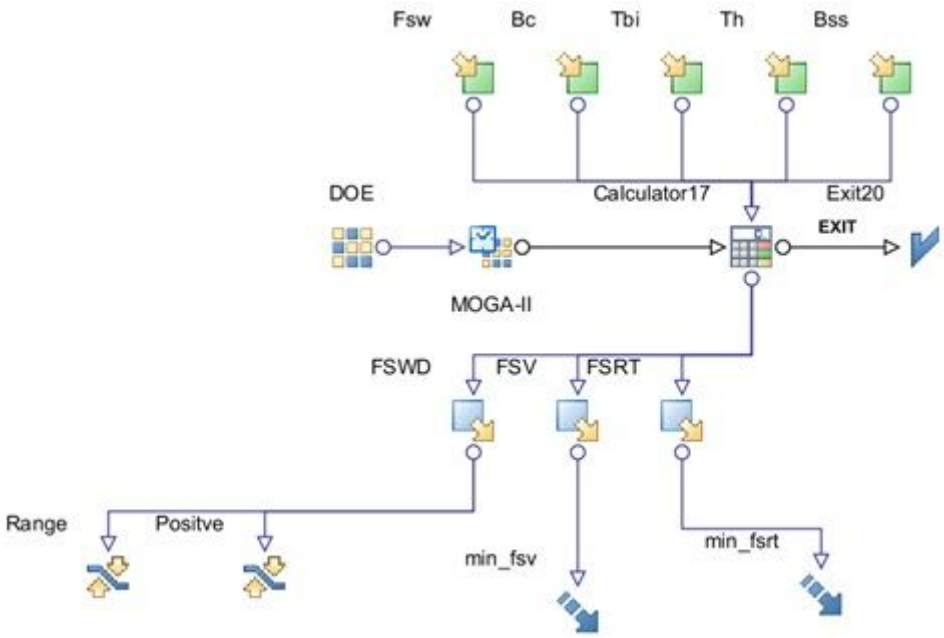

Figure 6

Optimization workflow using MOGA-II and RSM in modefrontier® software. MOGA-II is an efficient algorithm that uses a smart multi-search elitism. The algorithm attempts a total number of evaluations that are equal to the number of points in the DOE table (the initial population) multiplied by the number of generations.

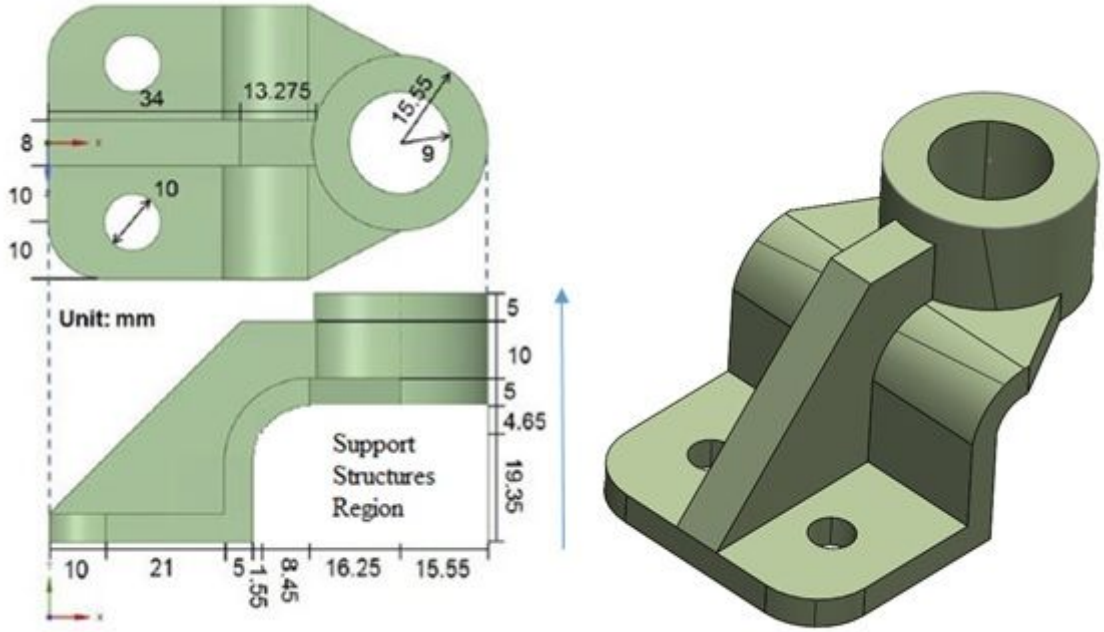

Figure 7

Bearing bracket specifications along with built orientation [18]

Figure 8

Bearing bracket fabricated with (a) default (b) optimum fragmeted support structures.

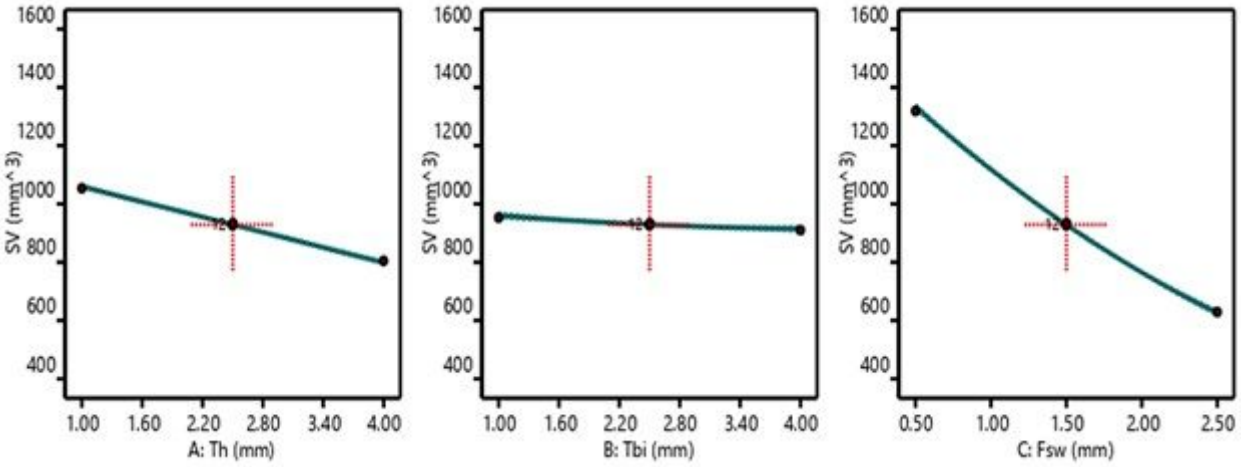

Figure 9

The main effects plots of fragmented support volume

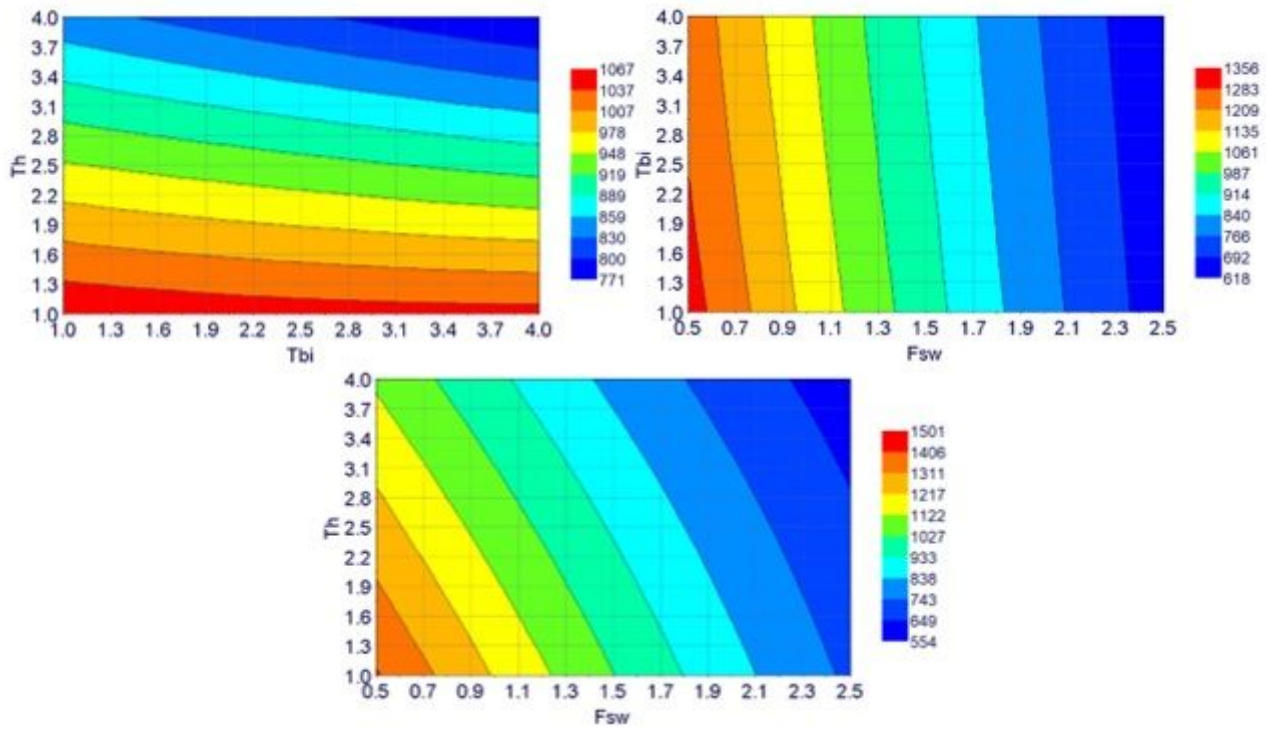

Figure 10

Contours plots showing the interaction of fragmented support parameters on fragmented support volume

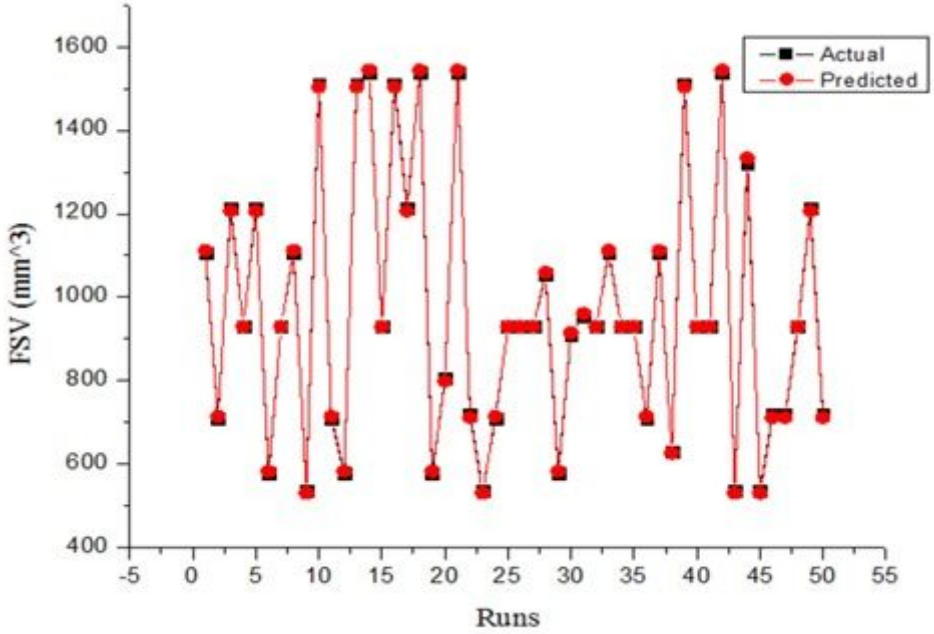

Figure 11

Comparison between actual and predicted values of fragmented support volume

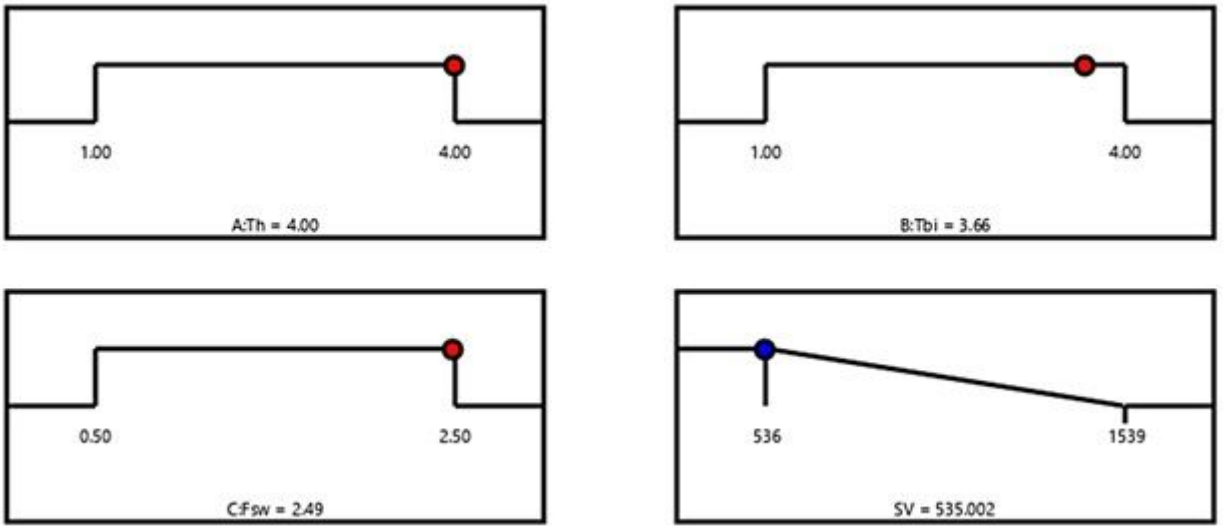

Figure 12

Selected optimal solution minimizing fragmented support volume based on desirability function

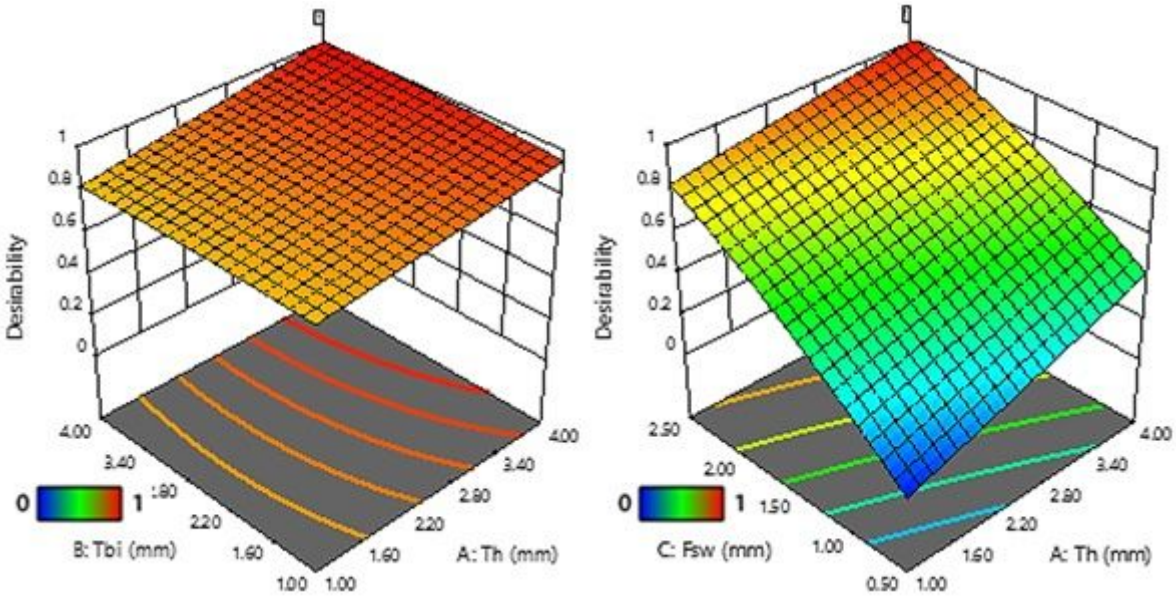

Figure 13

Variation of desirability function for fragmented support volume

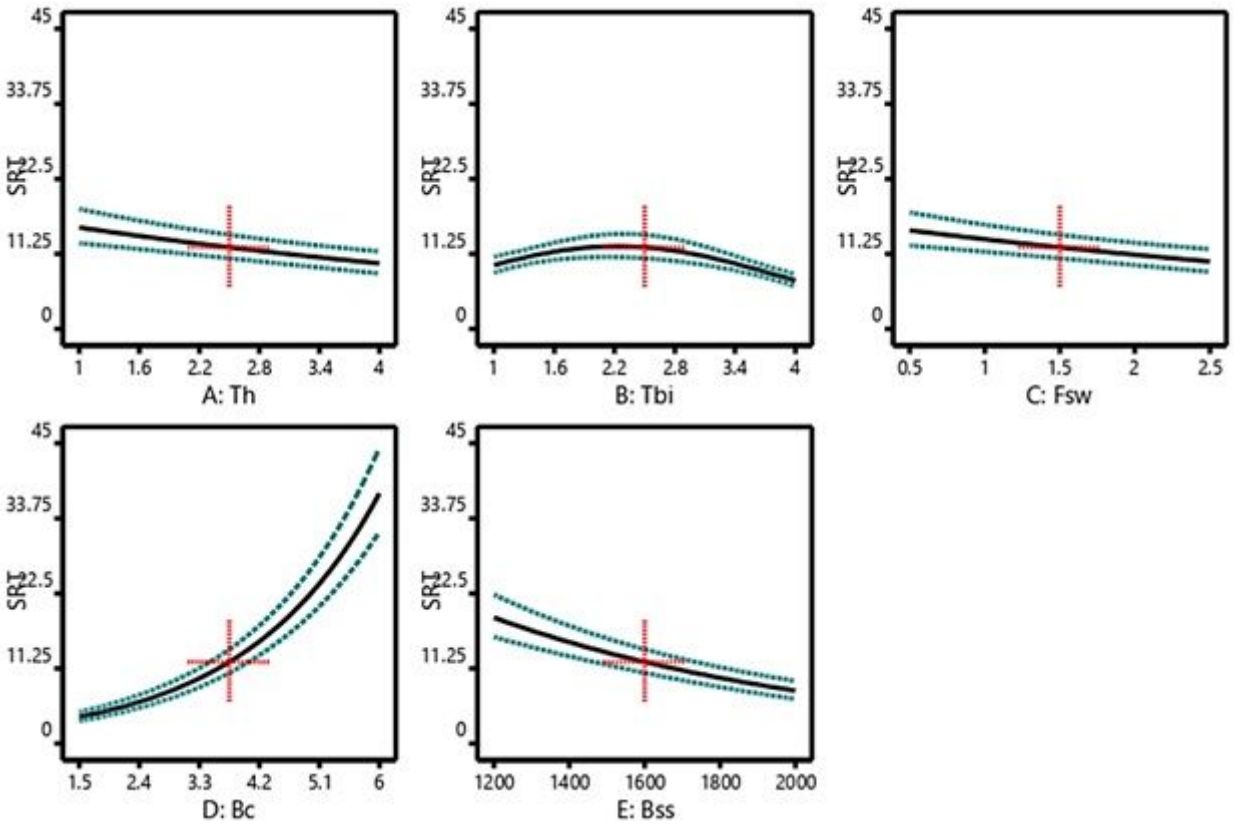

Figure 14

The main effects plots of fragmented support removal time

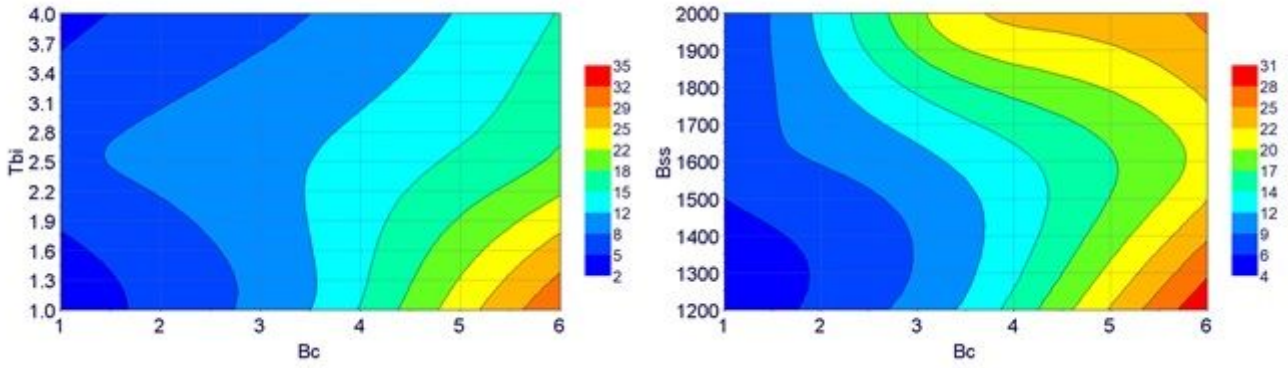

Figure 15

Contour plots showing the interaction of support parameters on fragmented support removal time

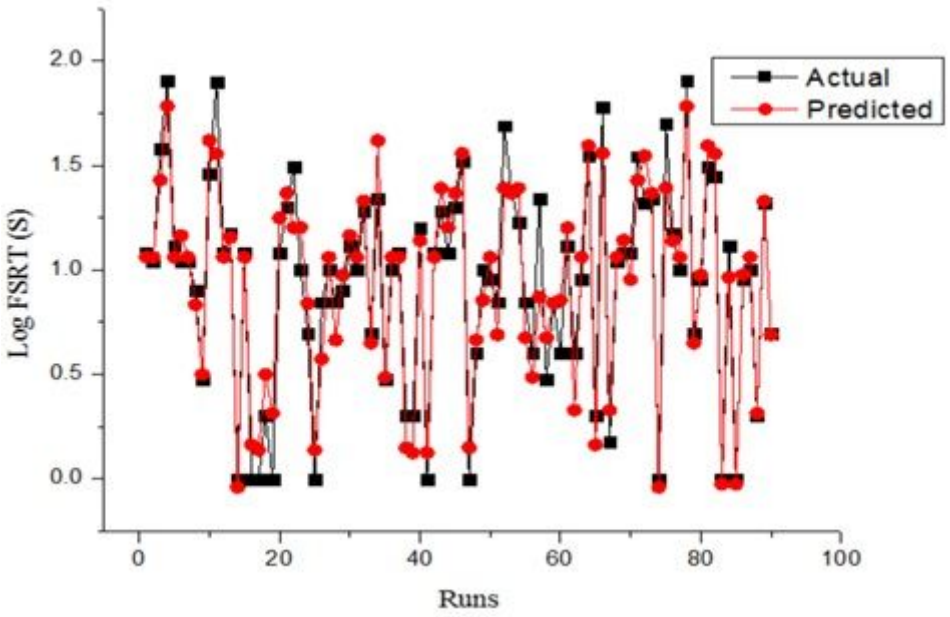

Figure 16

Comparison between actual and predicted values of Log FSRT

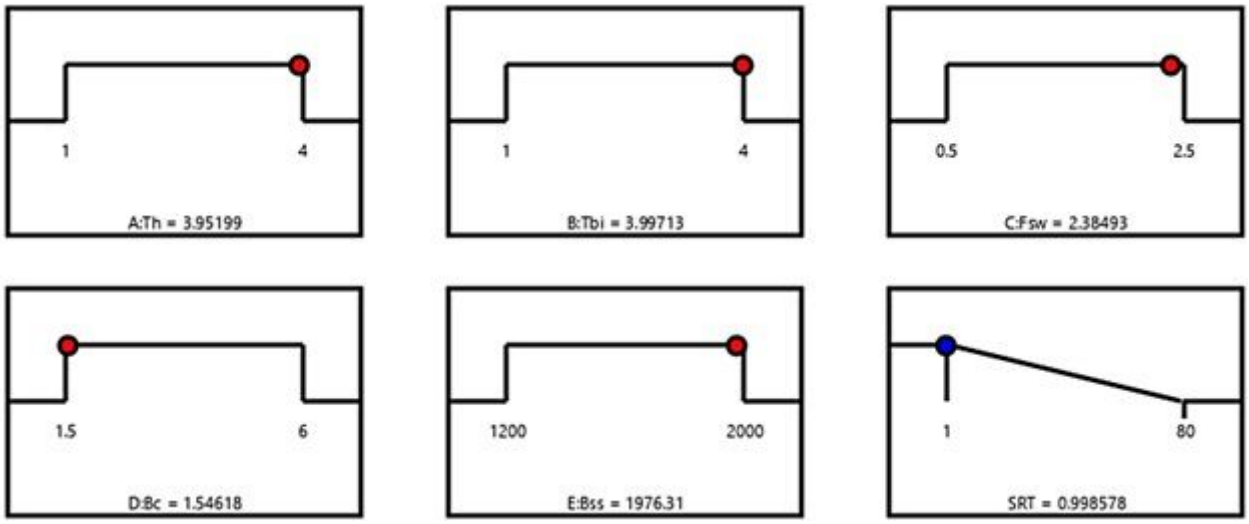

Figure 17

Suggested optimal solution minimizing fragmented support removal time based on desirability function

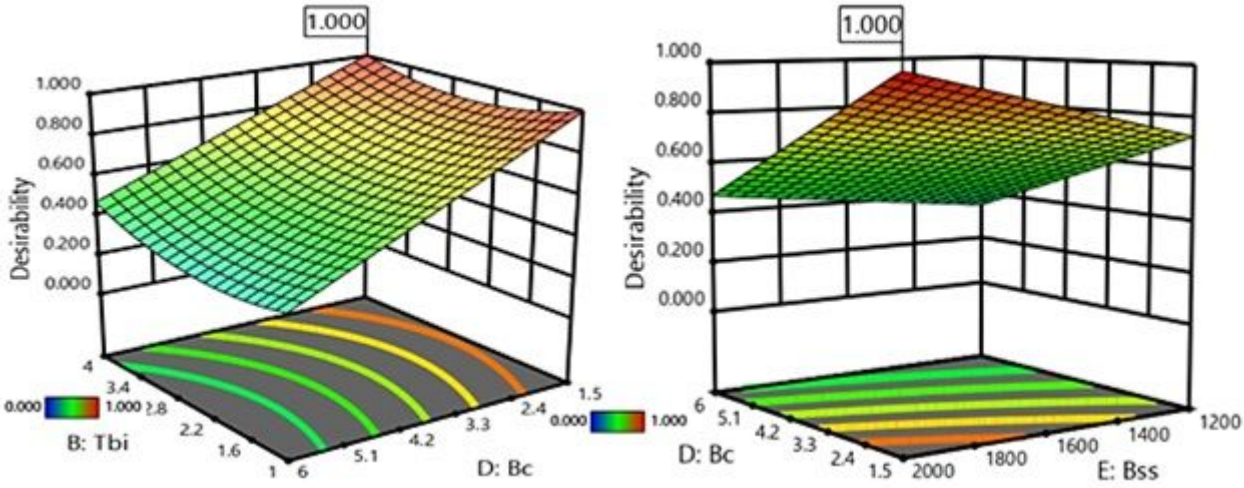

Figure 18

Variation of desirability function for FSRT

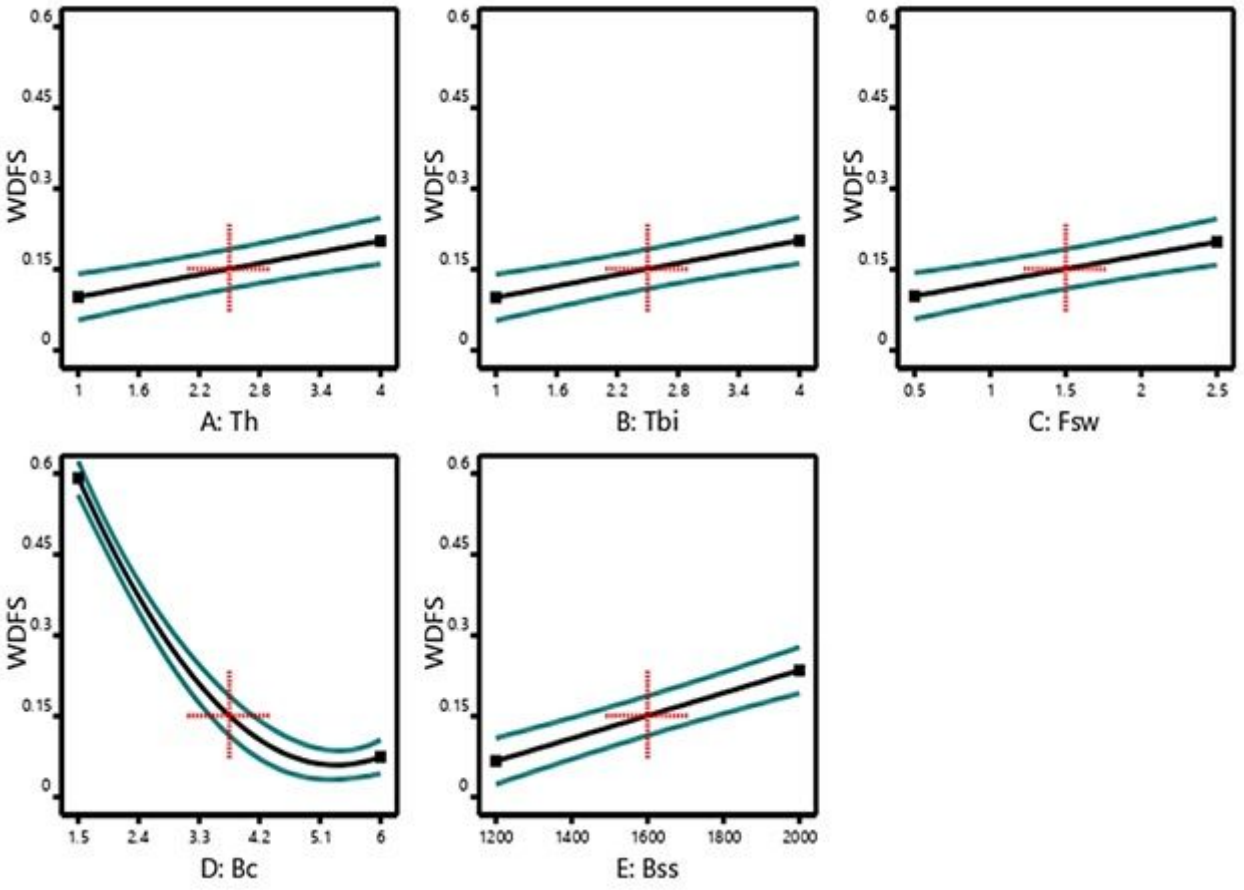

Figure 19

The main effects plots of warping deformation with fragmented supports

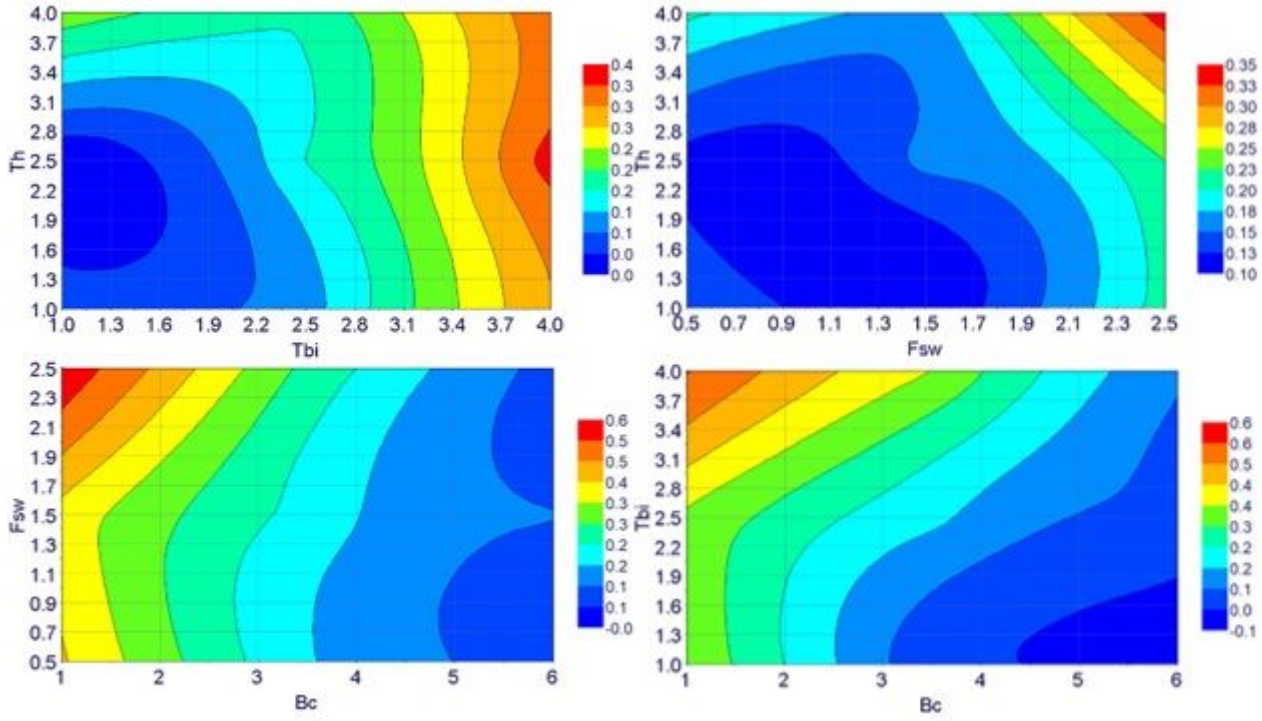

Figure 20

Contour plots showing the interaction of fragmented support parameters on warping deformation

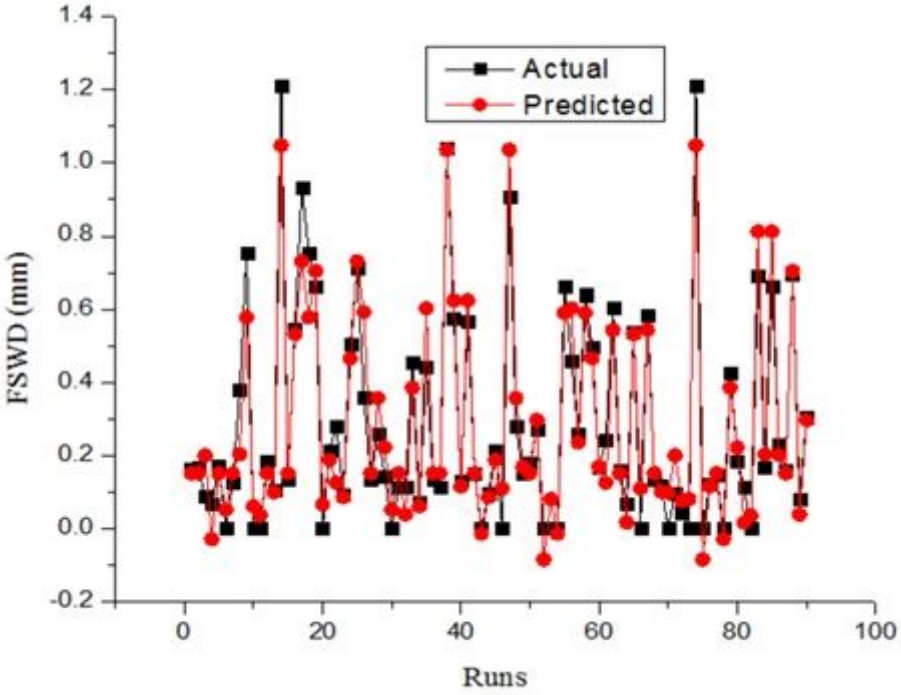

Figure 21

Comparison between actual and predicted values of warping deformation with fragmented support

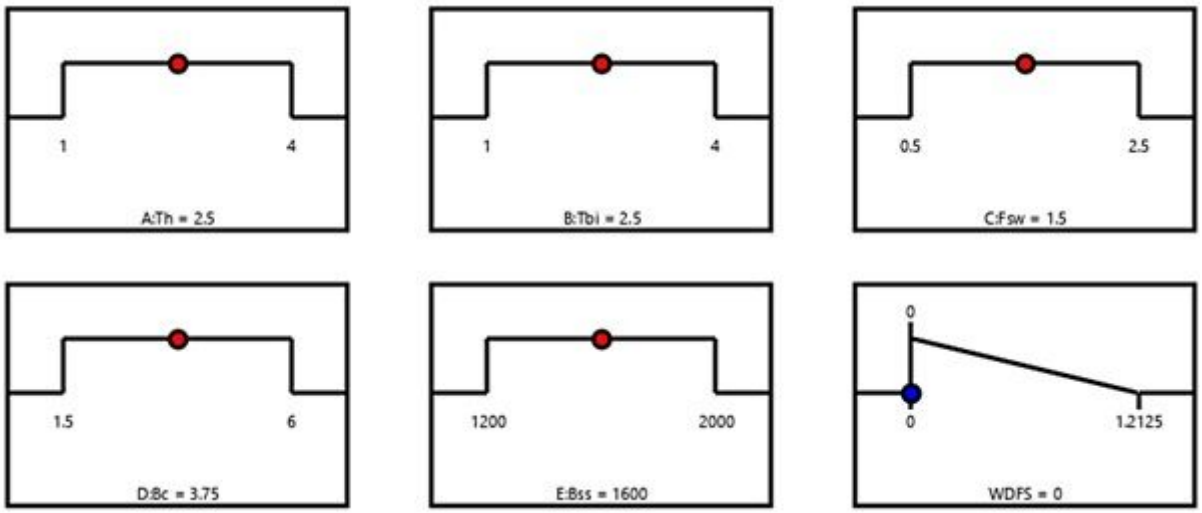

Figure 22

Selected optimal solution of warping deformation with fragmented support

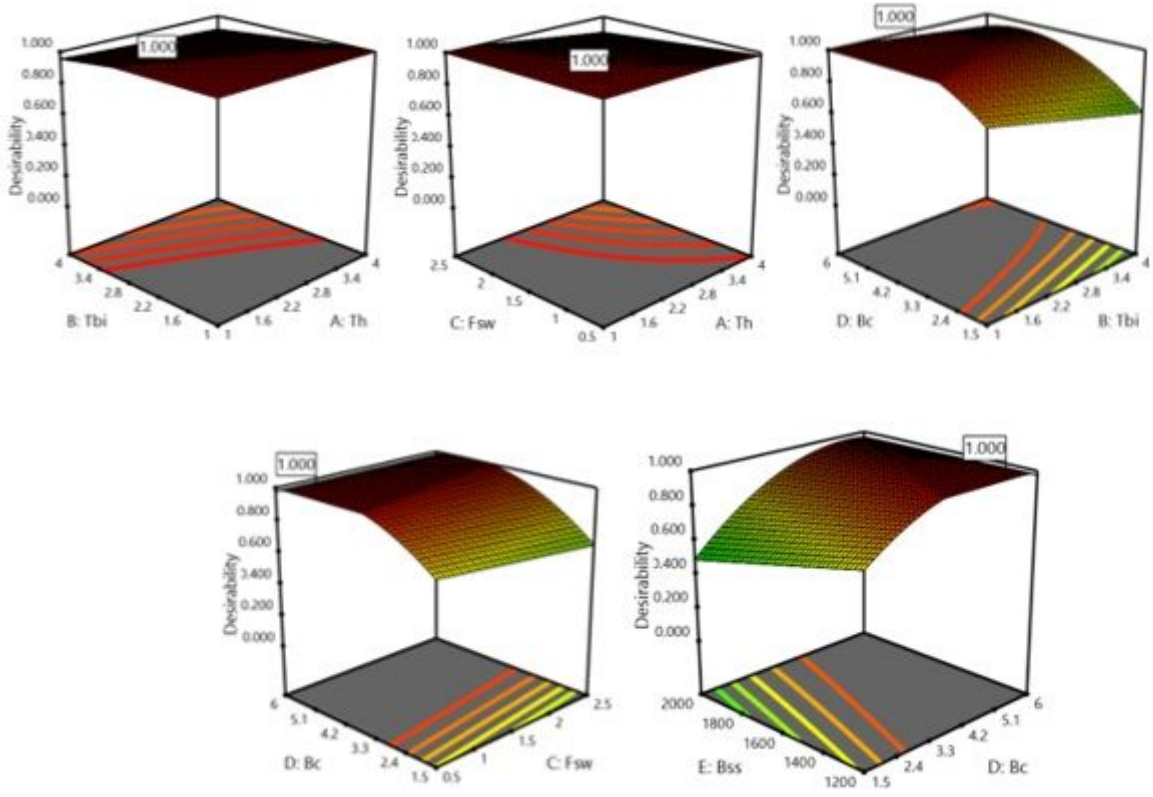

Figure 23

Variation of desirability function for warping deformation with fragmented support

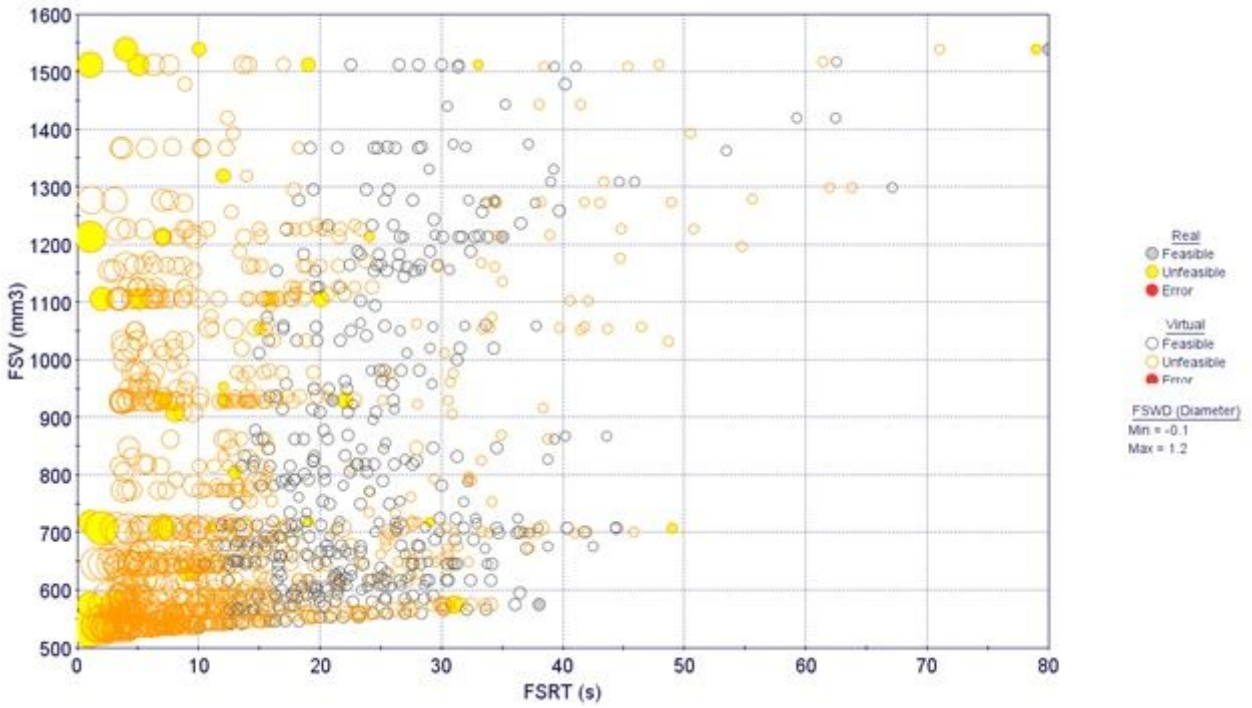

Figure 24

A 3D bubble chart of showing the complete design space

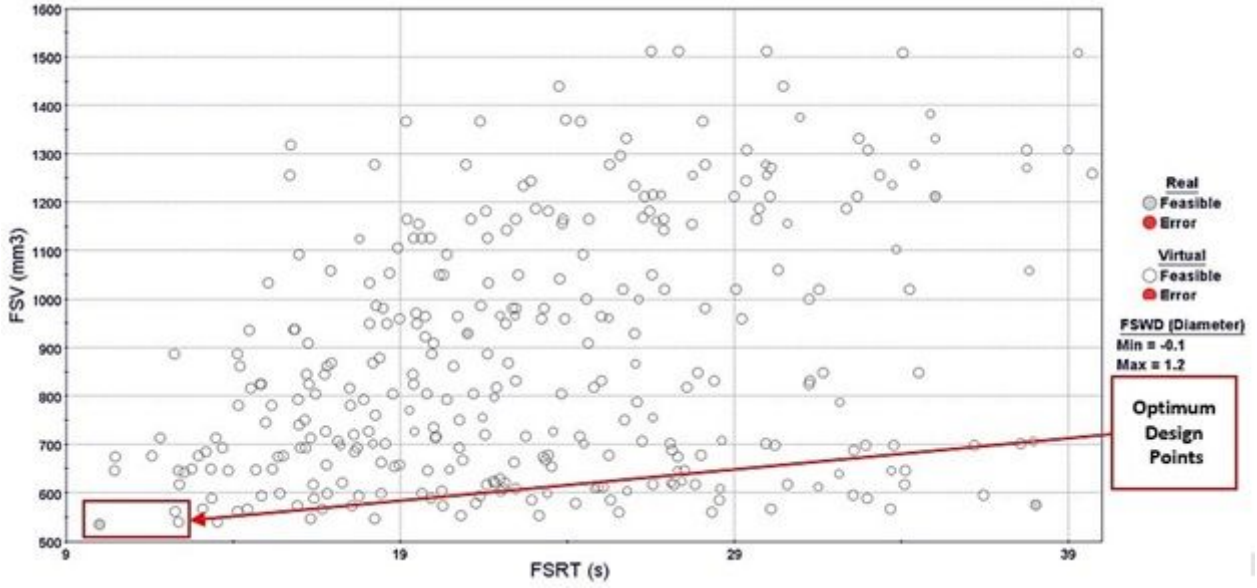

Figure 25

A 3D bubble chart of the feasible and optimum design points

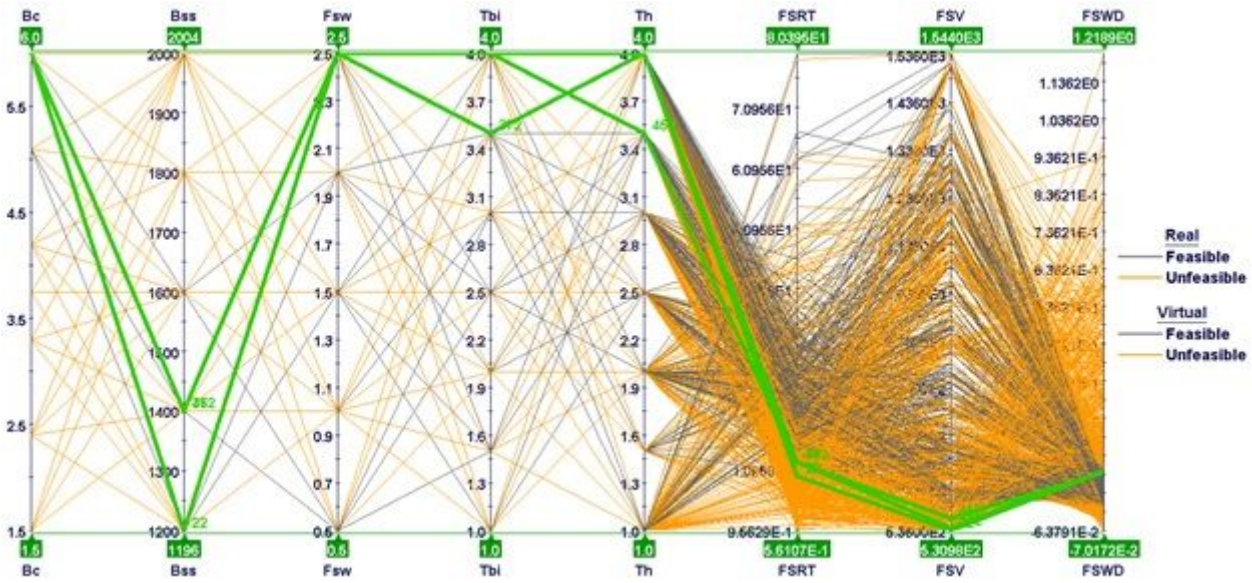

Figure 26

A parallel coordinate chart for the analysis of fragmented support parameters.

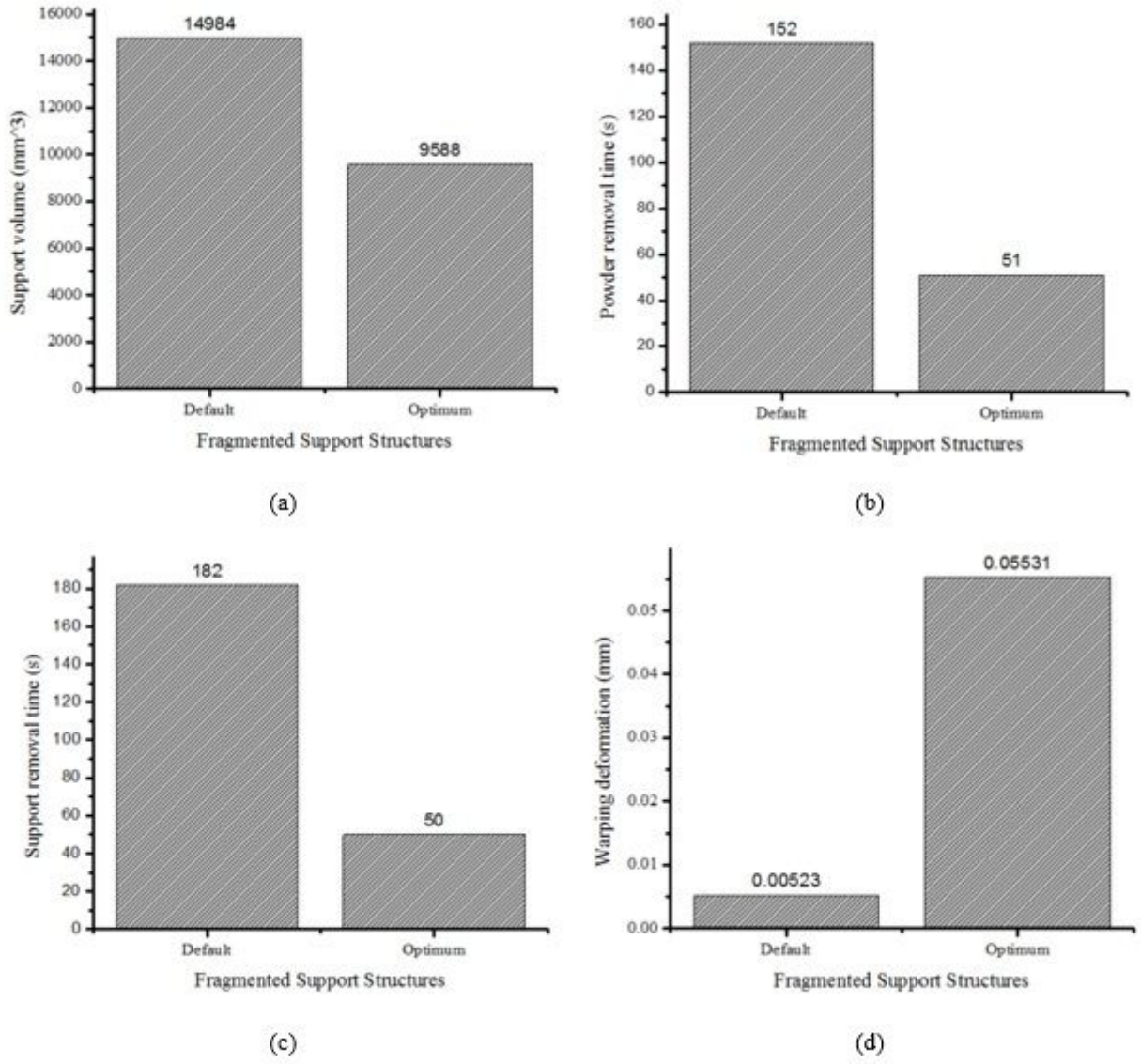

Figure 27

Comparison of performance measures for default and optimum parameters a) support volume b) un-melted powder removal time c) support removal time d) warping deformation.